Vol. 588: 29–42, 2018
https://doi.org/10.3354/meps12456

MARINE ECOLOGY PROGRESS SERIES
Mar Ecol Prog Ser

Published February 8

Modulation of the light field related to valve optical properties of raphid diatoms: implications for niche differentiation in the microphytobenthos

Johannes W. Goessling[1,*], Silja Frankenbach[2], Lourenço Ribeiro[3,4], João Serôdio[2], Michael Kühl[1,5]

[1]Marine Biological Section, Department of Biology, University of Copenhagen, Strandpromenaden 5, 3000 Helsingør, Denmark

[2]Centro de Estudos do Ambiente e do Mar (CESAM), Departamento de Biologia, Universidade de Aveiro, 3810-193 Aveiro, Portugal

[3]Centro de Ciências do Mar e Ambiente (MARE), Faculdade de Ciências da Universidade de Lisboa, Campo Grande, 1749-016 Lisboa, Portugal

[4]Université de Nantes, Mer-Molécules-Santé EA 2160, Faculté des Sciences et des Techniques, 2, Rue de la Houssinière, BP 92 208, 44322 Nantes, France

[5]Climate Change Cluster, University of Technology Sydney, Australia

ABSTRACT: Differences in the spectral light absorption of photopigments allow for niche differentiation and coexistence of cyanobacteria and diatoms. Evolution in the microphytobenthos could have further been shaped by the photonic crystal-like structures in the frustule of diatoms interacting with sunlight. We studied the optical properties in water of the valves of 3 pennate diatom species collected from an intertidal estuarine mudflat. We observed forward scattering of blue light in the valve, while the angle of incident white light at which this phenomenon was visible differed between the 3 tested raphid species. A slurry of oxidized frustules enhanced scalar irradiance in the blue spectral range by up to 120% compared to downwelling irradiance. Blue light induced higher relative electron transport rates at photosystem II and non-photochemical quenching compared to red actinic light. We hypothesize that structures in the pennate diatom frustule modulate microalgal light absorption for efficient photosynthesis and thereby contribute to niche differentiation of diatoms in the microphytobenthos.

KEY WORDS: Biological photonic structures · Epipelic diatoms · Photopigments · Chlorophyll fluorescence · Intertidal mudflats · Sediment light attenuation

Resale or republication not permitted without written consent of the publisher

INTRODUCTION

Diatoms are microscopic photosynthetic protists, present in the water column of oceans, in the benthos, intertidal habitats and many freshwater and moist terrestrial ecosystems (Vanormelingen et al. 2008). Due to their high abundance and diversity, diatoms are regarded as a very successful evolutionary group (Boyd et al. 2000, Thomas & Dieckmann 2002, Mock & Valentin 2004). This can partially be explained by efficient light use for photosynthesis in combination with effective photo-protection mechanisms (Ruban et al. 2004, Zhu & Green 2010), facilitating high diatom productivity in dynamic light environments (Mortain-Bertrand 1989, Lavaud 2007). Wave-focusing and shifting cloud cover can change solar irradiance locally within milliseconds (Schenck 1957, Max 1986). Spectral differences occur as a function of depth in the water column as influenced by suspended matter and water trophic states (Kirk

*Corresponding author: johannesg@bio.ku.dk

© Inter-Research 2018 · www.int-res.com

2010). Blue light may penetrate deep into oligotrophic waters, while longer wavelengths of the sunlight spectrum are attenuated e.g. by the inherent water absorption of red light and near-infrared radiation. Blue light attenuates more in turbid or nutrient-rich waters due to scattering and absorption of particulate and dissolved organic matter and absorption by phytoplankton (Atlas & Bannister 1980), which utilizes foremost blue and red wavelengths of the visible light spectrum (Gilbert et al. 2000). Diatoms inhabiting the microphytobenthos are exposed to a diffused light field caused by scattering on detritus, inorganic particles and organic matter (Baker & Lavelle 1984). Scattering of light affects both the intensity and quality of available photosynthetic active radiation (PAR) inside the sediment, while it can even enhance PAR locally (Kühl & Jørgensen 1994). In fine sediments, light of shorter wavelengths usually attenuates more due to scattering on densely packed small particles and light absorption by the microphytobenthos, but exhibits higher subsurface scalar irradiance maxima (Kühl et al. 1994, Cartaxana et al. 2016). Sedimentary light attenuation can be caused by Rayleigh scattering on subwavelength-sized particles, i.e. unconsolidated clay minerals like illite, kaolinite and montmorillonite (Babin et al. 2003), which are major constituents in intertidal mudflats (Bobos & Rocha 2006).

Diatoms contain large amounts of chlorophyll (chl) *a* and chl *c* for efficient light harvesting in the blue and red spectral range of light (Mann & Myers 1968). Carotenoids such as xanthophyll pigments expand the light absorption spectrum of diatoms towards the green wavelength range (Kuczynska et al. 2015). Carotenoids also shield against excessive radiation by heat dissipation under high irradiance; a mechanism that in diatoms is particularly effective under energy-rich blue light (Siefermann-Harms 1987). Phototrophic organisms evolved different mechanisms to cope with high solar irradiance, which can be roughly classified as removal and prevention strategies (Demmig-Adams & Adams 1992). Removal strategies include surveillance and scavenging of reactive oxygen species (Apel & Hirt 2004), photo electron circulation by sinks other than photosynthesis such as photorespiration (Wu et al. 1991), and dissipation of energy in the form of heat (Bilger & Björkman 1990). The xanthophyll cycle in diatoms is an effective mechanism to remove excessive energy (Schumann et al. 2007), enabling efficient regulation of photosynthesis under intermittent light regimes (Ruban et al. 2004). Prevention strategies involve structural adaptation that reduce of light exposure via reflection or attenuation of harmful radiation (Haupt 1973, Demmig-Adams & Adams 1992). Prevention strategies may also be mediated by structural features such as biological photonic crystal structures, e.g. it was demonstrated that specialized iridescent protein grana in the mantle of giant clams act as Bragg-reflectors back-scattering harmful radiation and reshaping the propagation of beneficial wavelengths for better exposure of their photosymbiotic microalgae situated in deeper tissue layers (Holt et al. 2014). While coloration of photopigments is based on selective light absorption, structural coloration is caused by the wave-nature of light leading to a specific interference pattern via diffraction gratings, selective mirrors or photonic crystals (Kinoshita et al. 2008, Sun et al. 2013).

A unique feature of diatoms is their encasement in a nanostructured silicate frustule, which has been shown to have photonic crystal-like properties (Fuhrmann et al. 2004) interacting with electromagnetic radiation in the ultra-violet (UV) to visible (VIS) spectrum of light (Ellegaard et al. 2016). The frustule comprises 2 valves and their corresponding girdle bands which keep the frustule together (Round et al. 1990). The term valve wall refers to the complex asymmetric 3D structures in the valve including chambers and pores of different size in the micro- to nanometer range (De Stefano et al. 2007, Chen et al. 2015, Romann et al. 2015, Valmalette et al. 2015). Diatoms can be classified by the shape and ornamentation of their valve, where centric valves show a radial symmetry and pennate valves are usually elongated with bilateral symmetric ornamentations (Round et al. 1990). Different functions have been proposed with regards to the frustule material properties and its micro- and/or nano-structure: (1) the complex architecture of the valve provides an enormous physical strength and could serve as predation defense (Hamm et al. 2003, Aitken et al. 2016); (2) the frustule might affect sinking rates in diatoms under nutrient depletion (Smetacek 1985); (3) the nanostructuring of the valve might sort nutrients from harmful bacteria and viruses by size exclusion (Losic et al. 2006); (4) the pH buffering property of biosilica enables the enzymatic conversion of bicarbonate to CO_2 inside the cell, thus enabling photosynthetic carbon assimilation (Milligan 2002); (5) the photonic crystal-like structures in the valve could modulate PAR for efficient photosynthesis (De Tommasi 2016), e.g. by focusing light onto the chloroplasts (De Stefano et al. 2007) or by screening incident light for harmful radiation and excess light energy (Yamanaka et al. 2008). In some diatom species, the biosilica

of the frustule itself absorbs UV light that could otherwise inhibit photosynthesis and damage the photosynthetic apparatus (Ellegaard et al. 2016). Mycosporine-like amino acids associated with the valve provide an additional UV-protection on the exterior side of the frustule (Ingalls et al. 2010). The photonic properties of frustules may be generated by different optical phenomena such as photonic waveguiding, Rayleigh scattering on single nanometric features of the frustule, diffraction on grating structures and Fabry-Pérot interference on the internal valve chamber walls (Hoover & Hoover 1970, Fuhrmann et al. 2004, Dossou 2017). However, the photonic crystal-like structures and frustule optics may significantly vary between the >100 000 described diatom species (Guiry 2012), and it is presently complicated to link frustule optical properties to the different life forms of diatoms, e.g. planktonic forms in surface waters, or non-motile and motile life forms inside the microphytobenthos. Only raphid diatoms are motile, due to a slit in their valve (the raphe), allowing for locomotion upon excretion of adhesive strands of mucilage (Edgar & Pickett-Heaps 1983).

In this study, we report on the frustule optical properties of different raphid diatom species from an estuarine intertidal mudflat. We describe the photosynthetic activity of this community as a function of light color and photon irradiance, and provide detailed information about the light attenuation characteristics in this particular environment. Motile raphid diatoms were extracted with the lens-tissue technique after induction of upwards migration with light and low-tide stimuli (Consalvey et al. 2004). Frustule optics were determined in different motile diatom species to evaluate whether differences in their frustule optics could affect niche differentiation inside the microphytobenthos.

MATERIALS AND METHODS

Sampling site

A meso-tidal mudflat was sampled at low tide during August and September 2016 on the Portuguese Atlantic Coast in the estuarine system 'Ria de Aveiro' (Portugal; 40° 35′ N, 8° 41′ W) (Serôdio et al. 2008). Sediment samples were transferred to polyethylene trays and kept at photon irradiances of 100 µmol photons m^{-2} s^{-1} provided as white light from a halogen lamp in 10 h light:14 h dark cycles. Sea water from the sampling site was added at the end of the light period and drained off again before illumination was started the next day. This cycle was repeated for 3 d after sampling.

Harvesting of motile diatom species, preparation of rinsed frustules and taxonomic identification

Sediment from the intertidal mudflat was brought to the laboratory, where motile raphid diatom species were sampled for the experiments within 3 consecutive days. Immediately after the onset of illumination in the morning, a lens cleaning tissue (WhatmanTM, GE Healthcare) was placed on the sediment surface to collect motile cells. The lens tissue was removed after 2 to 4 h and washed in autoclaved seawater, and the resulting suspension was stored for subsequent photophysiological characterization. Diatom suspensions were further collected for extraction of oxidized frustules. For this, the diatom suspension was centrifuged at 5000 × *g* prior to removal of organic matter by nitric acid oxidation, which was monitored by the fading color of bromophenol blue added to the suspension. Cleaned diatom frustules were washed in distilled water before a drop of the solution was placed on a coverslip and mounted in NaphraxTM (Northern Biological Supplies, UK). Taxonomic identification and cell counts were done at 100× using an oil immersion objective on a Leica DM2500 LED microscope equipped with differential interference contrast (DIC). A total of 40 random ocular fields were screened, and 668 valves were counted. Species were identified according to Witkowski & Lange-Bertalot (2000) and references therein.

Scanning electron microscopy

Rinsed valves from the diatom suspension were air dried on metal stubs covered with a thin pellicle of graphite, coated with gold-palladium and observed with a scanning electron microscope (JEOL-JSM 5400, Jeol, Tokyo), operated at 10 to 20 kV.

Hyperspectral imaging and image analysis

A water drop containing cleaned diatom frustules was transferred to a microscope glass slide and covered with a glass cover slip. Transmittance was measured with an objective with 10× magnification (UPlanFL N 10×/0.3; Carl Zeiss, Germany) on a light microscope (Axiostar Plus, Carl Zeiss) connected to a hyper-spectral camera system (VNIR-100, Thermis

Vision Systems, St Louis, USA). Hyperspectral images were calculated in percent transmission, after correction for dark noise and normalization to full light transmittance images acquired in the absence of samples. Light transmittance was determined on a ~10 μm^2 area on the valve surface. Data acquisition from hyperspectral image stacks was performed with the PhiLumina Hyperspectral Imaging System software (PhiLumina, University of Mississippi, USA).

Dark field microscopy

Cleaned valves from the suspension were observed in a drop of water with an optical compound microscope (BX41 Laboratory Microscope, Olympus, USA) at 40× or 200× magnification (UPlanFL N 4×/NA = 0.13; UPlanFL N 20×/NA = 0.5; Carl Zeiss). Dark stops of different size were applied between light source and condenser (U-PCD2, Olympus, Tokyo) to generate different angles of incident white light, i.e. θ = 15°, θ = 25°, and θ = 50°. Images were recorded with a charge coupled device camera using the manufacturers' software (Color View Soft Imaging System, Olympus).

Variable chlorophyll fluorescence imaging

A 1 ml portion of diatom suspension was incubated with 1 µl of 0.25 µM latrunculin-A (LAT-A) solution (Thermo Scientific, Waltham, USA). It was earlier demonstrated that LAT-A inhibits motility of raphid diatoms, without affecting photosynthesis (Cartaxana & Serôdio 2008). A drop of inhibited diatom suspension was placed on a microscope glass slide and covered with a glass coverslip. The coverslip was mounted on an epifluorescence microscope (Axiostar Plus, Carl Zeiss) equipped with a variable chlorophyll fluorescence imaging system (RGB Microscopy I-PAM, Heinz Walz, Germany; Trampe et al. 2011). Keeping the sample in the dark, blue non-actinic measuring light (λ = 450 nm) was used to determine minimum fluorescence yields (F_o), while a strong saturating blue light pulse was used to determine the maximum fluorescence yield in the dark (F_m). Data were recorded using the I-PAM system software (ImagingWin; Heinz Walz), while subsequent calculations were done on exported image files of F_o and F_m (in TIF format). Variable fluorescence (F_v) was calculated as $F_v = F_m - F_o$ (Maxwell & Johnson 2000), prior to calculation of the maximum quantum yield of PSII (ϕ_{PSII}; Genty et al. 1989) as $\phi_{PSII} = F_v/F_m$, using the Ratio Plus plug in and image calculator functions of the freeware Fiji (ImageJ) (Schindelin et al. 2012).

PSII absorption cross section and steady state light curves of PSII electron transport vs. irradiance

The functional wavelength-dependent light absorption cross section of PSII ($Sigma_\lambda II$) and the effective PSII quantum yield ($\Delta F/F_m'$) were quantified with a multicolor variable chlorophyll fluorescence analyzer (Multi-Color PAM; Heinz Walz). $Sigma_\lambda II$ was measured at monochromatic light as provided by LEDs at wavelengths of λ = 440, 480, 540, 590, and 625 nm. Measurements were performed with the script file Sigma1000.FTM executed in the firmware PamWin_3.Ink as described by Schreiber et al. (2012). Thereafter, diatom suspensions diluted in autoclaved seawater in the assemblage presented in Table 1 were dark-acclimated for 30 min before steady state light curves were derived from measurements of the $\Delta F/F_m'$ over a set of increasing actinic irradiance levels. Photon irradiance levels of 15, 45, 100, 200, 250, 350, 530, 770, 1050 and 1800 µmol photons m^{-2} s^{-1} of actinic blue light (λ = 440 nm) or 10, 40, 100, 200, 360, 550, 800, 1100, and 1800 µmol photons m^{-2} s^{-1} of actinic red light (λ = 625 nm) were applied for each 12 min prior to saturation pulse measuring $\Delta F/F_m'$. Photosynthetic electron transport rates at PSII (ETR_{II}) were calculated under consideration of $Sigma_\lambda II$ for the respective colors (Schreiber et al. 2012) as described elsewhere (Genty et al. 1989, Maxwell & Johnson 2000). Non-photochemical energy quenching (NPQ) at PSII was calculated as described by Bilger & Björkman (1990).

Modification of the multicolor PAM measurement head

The measuring head unit of a multicolor PAM (MCP-BK Optics, Heinz Walz) was modified to allow for simultaneous illumination of sediments with colored light, while measuring scalar irradiance depth profiles with a fiber-optic microprobe. A 3D model of the MCP-BK Optics unit was generated in the open source software Autodesk 123D design (Autodesk, Mill Valley, USA) using the dimensions provided in the multicolor PAM manual. In the modified version, an open space was left close to the measuring window. Consequently, a fiber optic scalar irradiance microprobe could be inserted into the sediment, while the same spot could be illuminated with the

Table 1. Diatom taxa collected from an estuarine intertidal mudflat (Aveiro, Portugal). The taxa are listed in alphabetical order with the 3 most abundant species marked by grey shading

Taxon	Abundance (%)	Rank
Amphora sp.1	8	12
Amphora sp.2	0.15	12
Amphora sp.3	0.3	11
Entomoneis sp.1	0.15	12
Fallacia sp.1	0.15	12
Gyrosigma fasciola (Ehrenberg) J. W. Griffith & Henfrey	31.89	1
Navicula cf. phyllepta Kützing	3.89	7
Navicula gregaria Donkin m.2	4.79	6
Navicula phyllepta Kützing	0.45	10
Navicula salinarum Grunow cf	0.15	12
Navicula sp.1	5.84	4
Navicula sp.2	17.37	3
Navicula sp.3	3.29	8
Navicula sp.4	0.45	9
Navicula sp.5	0.15	12
Nitzschia frustulum (Kützing) Grunow	0.3	11
Nitzschia pararostrata (Lange-Bertalot) Lange-Bertalot	0.15	12
Nitzschia sp.1	0.3	11
Staurophora salina (W. Smith) Mereschkowsky	4.49	5
Staurophora sp.1	25.45	2
Tryblionella apiculata Gregory	0.15	12

PAM emitter rod of the unit (see Fig. S1 in Supplement 1 at www.int-res.com/articles/suppl/m588p029_supp/). The 3D printed model was made out of PLA nylon filament (Nylon Black, BEEverycreative, Aveiro, Portugal) in a full metal dual extruder (model helloBEEprusa, BEEverycreative). More detailed information on how to use this 3D printer is published elsewhere (Serôdio et al. 2017). The modified 3D model produced in the software Autodesk 123D design is available in Supplement 2.

Scalar irradiance in sediments with or without diatoms, and in suspensions of oxidized diatom frustules

Autoclaved sediment was muffled in an incubator at 70°C for 3 d. Thereafter, sediment was filled into 50 ml tubes and left overnight until saturated with (1) autoclaved seawater or (2) diatom suspension extracted from the intertidal sediment in the assemblage presented in Table 1. Attenuation of scalar irradiance was measured with a fiber optic scalar irradiance microprobe (Rickelt et al. 2016) inserted into the sediment surface at an angle of 45° relative to the vertically incident light. Surface positioning of the sensor was controlled by observation through a digital 400× microscope (Dino-Lite AM4013MZT4, Electronics Corporation, USA). The sensor was inserted into the sediment in vertical increments of 0.1 mm using a micromanipulator (MM33, Märtzhäuser, Germany) controlled by an electric motor (Model 18011 Controller, Oriel Encoder Mike and Oriel, Oriel Newport Corporation, USA). Downwelling spectral irradiance (Ed) (λ = 400–800 nm) from a halogen lamp (KL 2500 LCD, Schott AG, Jena, Germany), or from a modified multicolor PAM LED panel (see description above; determined at wavelength λ = 440 and 625 nm, respectively) was recorded with the scalar irradiance microprobe connected to a PC-controlled spectrophotometer (USB 2000+, Ocean Optics, Dunedin, USA) running the manufacturer's spectral acquisition software (Spectra Suite, Ocean Optics). Scalar irradiance spectra measured at different depths below the sediment surface were normalized to the incident downwelling irradiance spectra measured over a black light well, i.e. a black taped box. The same setup was used to measure scalar irradiance spectra in a mix of densely packed oxidized frustules in the species assemblage presented in Table 1 in a droplet of water, where the measurements were subsequently normalized to scalar irradiance spectra measured in a droplet of water in the absence of frustules (see Fig. 6B).

Statistical analysis

Significance was determined at the $p < 0.05$ level using 1-way analysis of variance (ANOVA) followed by the Holm Sidak post-hoc test. Significant differences of $Sigma_{\lambda}II$ were tested on the effects of different wavelengths, i.e. λ = 440, 480, 540, 590 and 625 nm. Significant differences of light attenuation in sediments were tested at wavelengths of λ = 440 nm and λ = 625 nm at different depths. Significant differences of scalar irradiance in mixed oxidized frustules were tested at wavelengths λ = 440 nm and λ = 625 nm on one level, i.e. scalar irradiance in percent of incident irradiance. All data were normally distributed and passed the equal variance test. Degrees of freedom are indicated as subscript letters after *F* val-

ues, while results from the post-hoc test are indicated as statistical power (p)-values. All statistics were performed with SigmaPlot 11.0 (Systat Software).

RESULTS

Composition of raphid diatoms in the microphytobenthos

The silicate valves of raphid diatom species bear a raphe slit facilitating motility by excretion of mucilage (Fig. 1). The raphid fraction of diatoms extracted from an estuarine intertidal mudflat was dominated by the species *Gyrosigma fasciola* (32%), *Staurophora* sp.1 (25%) and *Navicula* sp.2 (17%). In total, 21 species with an abundance of >0.15% were identified. The large diatom species *Gyrosigma balticum* and *Pleurosigma angulatum* were very rare (<0.15%), but an examination of a permanent sample slide at lower magnification (200×) confirmed that they were an integral part of the diatom assemblage (Table 1).

Spectral light transmittance through single valves of raphid diatoms in water

Transmittance spectra through valves of the species *G. balticum* and *P. angulatum* in water showed stronger attenuation of shorter wavelengths, when an objective with lower numerical aperture (NA = 0.14) was used. This was not the case in the most abundant species *G. fasciola*, which appeared almost transparent in hyperspectral imaging in the same optical setup (exemplary spectra; Fig. 2B). Pore struc-

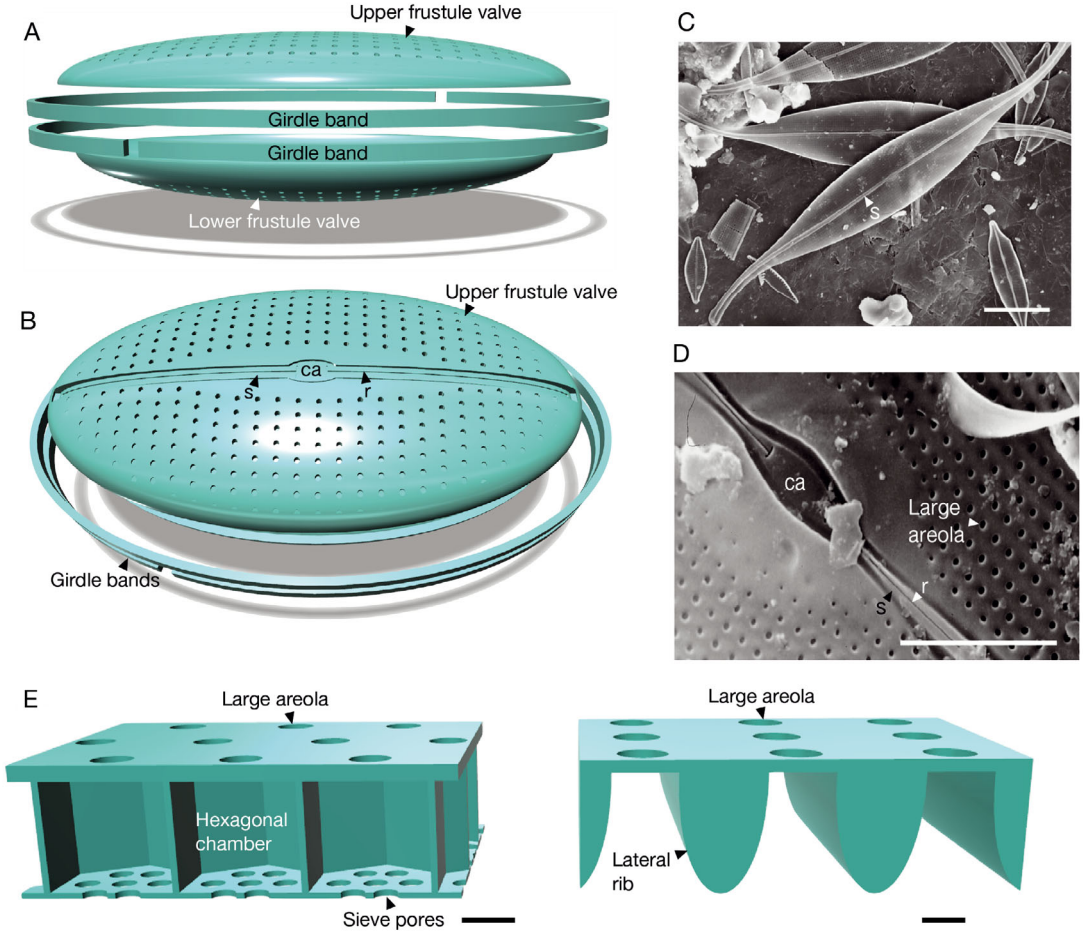

Fig. 1. Organization of the frustule of motile raphid diatoms. Raphid frustule scheme in (A) lateral view and (B) distal view. (C) SEM image of the raphid pennate diatom species *Gyrosigma fasciola*. (D) Close-up on the exterior surface of the *Gyrosigma fasciola* valve observed in SEM. (E) Illustration of the valve wall nanostructure variety in cross-section showing hexagonal arrangement (left hand; inspired by centric *Coscinodiscus* spp.) and rib structures with areolae in square lattice arrangement (right hand; inspired by pennate *Achnanthes* spp.). Abbreviations: Central area (ca); sternum (s); raphe (r). Scale bars = 5 µm (C,D); ~500 nm (E)

turing on the exterior side of the valve surface differed in lattice pattern between the 3 tested species, i.e. areolae of *G. fasciola* valves were arranged in square lattice, *G. balticum* in quasi-square and *P. angulatum* in a hexagonal arrangement (Fig. 2C).

Light scattering properties of single valves of raphid diatoms in water

In dark field microscopy, forward scattering of blue light was observed on valves of *G. fasciola*, *G. balticum* and *P. angulatum*. However, the angle of incident white light (θ) at which this phenomenon was visible differed between the species. Forward scattering of blue light was visible at incident light angles of θ = 50° on valves of *G. fasciola* and *P. angulatum* and at incident light angles of θ = 15° and θ = 25° on valves of *G. balticum* (Fig. 3A). Although other coloration was possible at different angles, e.g. greenish coloration on the valves of *G. balticum* at a θ = 50° angle of incidence, forward scattering of blue light was the most abundant observation in all tested species (Fig. 3A).

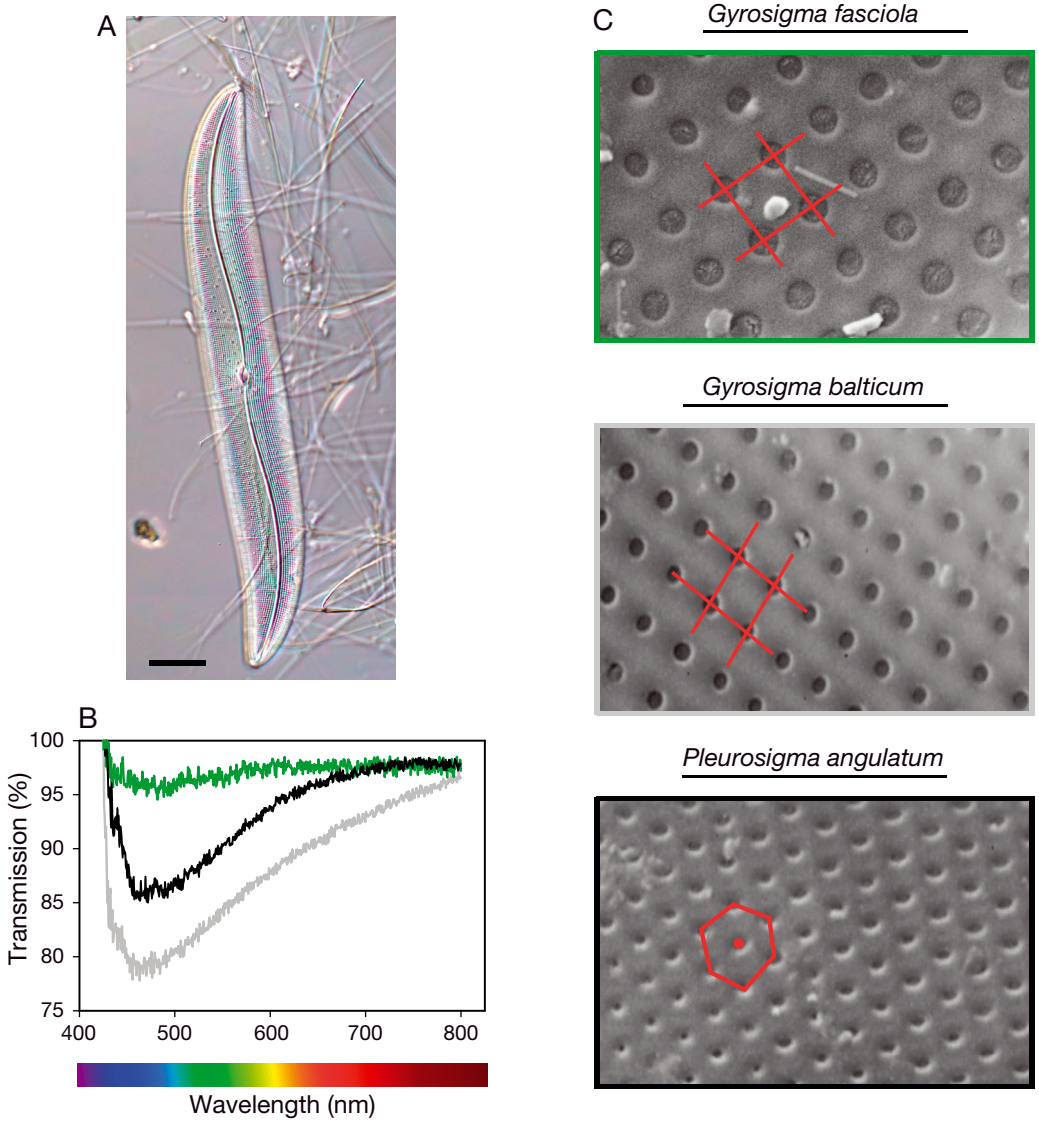

Fig. 2. Structural coloration of valves in raphid diatoms. (A) Micrograph of *Gyrosigma balticum* in differential interference contrast microscopy. (B) Transmission spectra of single valves of *Gyrosigma fasciola* (green), *Gyrosigma balticum* (grey) and *Pleurosigma angulatum* (black) observed with hyperspectral imaging. (C) SEM images of the corresponding species showing the arrangement of large areolae on the exterior valve side indicated in red color. *Gyrosigma fasciola*: square arrangement; *Gyrosigma balticum*: quasi-square arrangement; *Pleurosigma angulatum*: hexagonal arrangement with a central pore. Scale bars = 20 µm (A); 1 µm (C)

Spatial distribution of photosynthesis in diatom cells

Differences between the 3 diatom species were also observed in the distribution of chloroplasts at the single cell level, as determined with a microscope imaging variable chlorophyll fluorescence. We observed differences in the cellular spatial distribution of maximum quantum yields of PSII (ΦPSII). In cells of *G. fasciola*, ΦPSII was distributed in bilateral symmetry about the apical plane. Cells of *G. balticum* hosted a single large chloroplast filling almost the entire cell in close proximity to the frustule. Cells of *G. balticum* hosted 2 clearly defined chloroplasts (Fig. 3B).

Photosynthesis activity of raphid diatoms in suspension

Light color significantly affected the functional wavelength-dependent absorption cross-section of PSII ($Sigma_\lambda II$; $F_{4,14}$ = 33; $p < 0.001$). $Sigma_\lambda II$ was maximal at λ = 440 nm with 6.6 ± 0.6 nm^2, followed by λ = 480 nm with 4.8 ± 0.7 nm^2 and 3.4 ± 0.5 nm^2 at λ = 590 nm (n = 5; mean ± SD). $Sigma_\lambda II$ was lowest at λ = 540 nm with 2.2 ± 0.3 nm^2 and λ = 625 nm with 2.7 ± 0.6 nm^2 (Fig. 4A).

Blue light (λ = 440 nm) induced highest ETRII of 320 ± 23 µmol electrons m^{-2} s^{-1} at an irradiance of 750 µmol photons m^{-2} s^{-1}, while red light (λ = 625 nm) induced ETRII of 213 ± 13 µmol electrons m^{-2} s^{-1} at

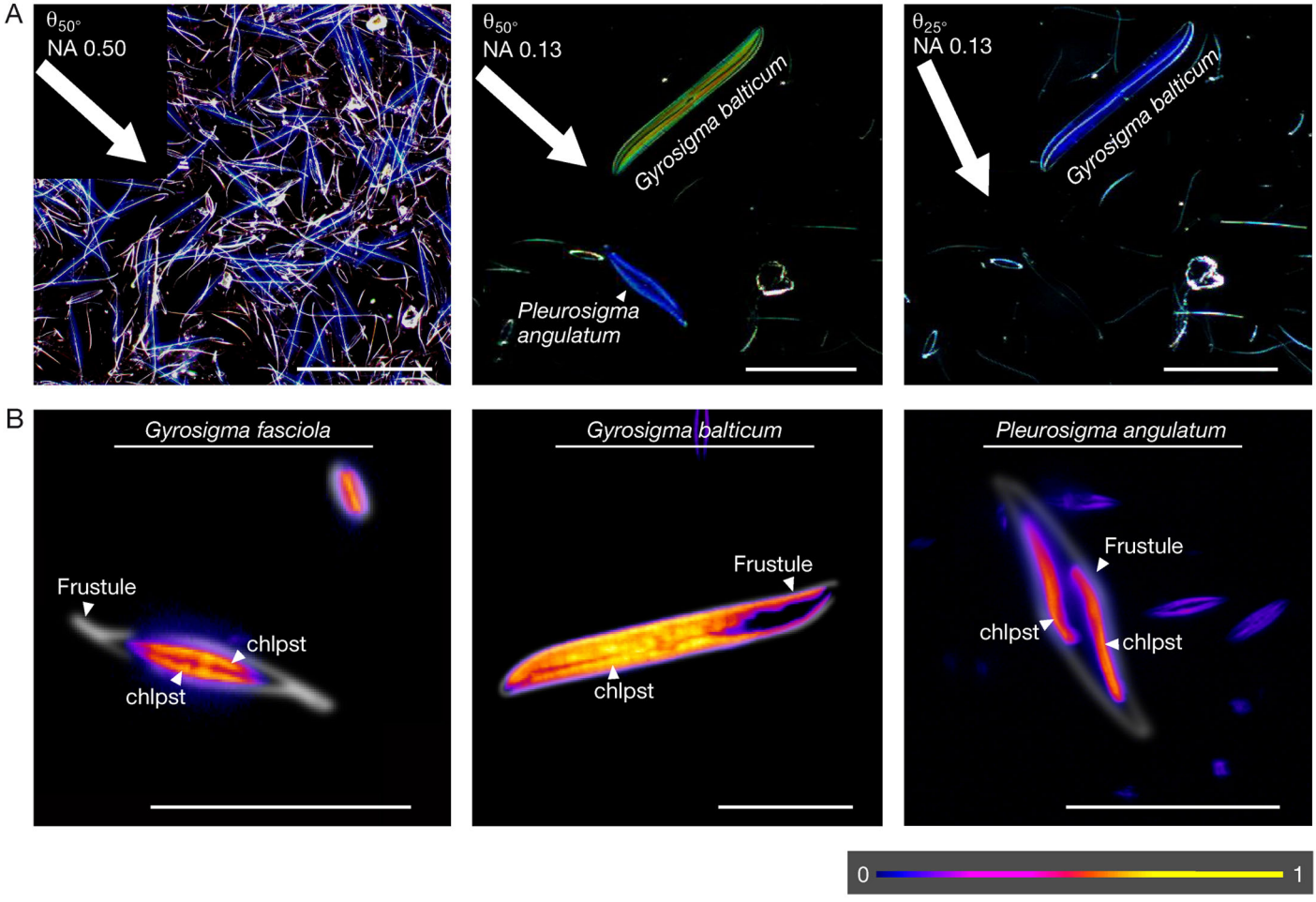

Fig. 3. Optical properties of valves and *in vivo* distribution of photosynthesis. (A) Light scattering properties of valves in water observed with objectives of different numerical aperture (NA) in dark field microscopy. The center and right hand image shows the same field of view at different angle of incidence (θ) varied with dark stops of different size. (B) Distribution of the maximum quantum yield of PSII (see color bar for scale) in *Gyrosigma fasciola*, *Gyrosigma balticum* and *Pleurosigma angulatum*, as observed by variable chlorophyll fluorescence microscopy (Trampe et al. 2011). The spatial arrangement of chloroplasts (chlpst) and the frustule outlines are indicated. Scale bars = 100 µm (A,B)

an irradiance of 1600 µmol photons m^{-2} s^{-1} (n = 3; mean ± SD; Fig. 4B). Non-photochemical energy quenching (NPQ) at photosystem II was higher under blue light compared to NPQ determined at comparable photon irradiances of red light (n = 3; Fig. 4C).

Scalar irradiance in sediments in the absence and presence of live diatoms

Sediments from an intertidal estuarine mudflat were first autoclaved to determine scalar irradiance (E_0) and light attenuation in the absence of live diatoms and cyanobacteria. Depth attenuation of blue light (λ = 440 nm) was significantly higher compared to that at red light (λ = 625; n = 3; $F_{1,53} = 37$; $p < 0.001$; Fig. 5A). When diatoms were spiked into the autoclaved sediment, attenuation of shorter wavelength in the tested range λ = 450–800 nm increased. In addition, attenuation in the red spectral range maximum at λ = 664 nm was observed (n = 3; Fig. 5B). When normalizing scalar irradiance spectra (E_0) measured at 0.1 mm depth in sediments spiked with diatoms to similar measurements in autoclaved sediment, a typical diatom light absorption spectrum was calculated. The same light absorption profile was determined in the diatom suspension (n = 3; Fig. 5C).

Scalar irradiance in a water drop containing mixed frustules from raphid diatoms

The presence of frustules from raphid diatoms significantly enhanced scalar irradiance (in % of incident irradiance) at shorter wavelengths (~1.3-fold) compared to that of longer wavelength light, i.e. E_0 at λ = 440 was 117 ± 8%, while E_0 was 91 ± 5% at λ = 625 (n = 9; mean ± SD; $F_{1,19} = 77$; $p < 0.001$; Fig. 6).

DISCUSSION

While diatom frustules usually appear transparent in light microscopy when an objective with large numerical aperture is used (Hoover & Hoover 1970; Fig. 2A), we observed attenuation of light in the blue spectral range in valves of *Gyrosigma balticum* and *Pleurosigma angulatum* when using lower numerical aperture objectives. This differed from the valves of the main abundant species *Gyrosigma fasciola*, which appeared transparent throughout the visible spectrum of light (Fig. 2B). Variation in the valve pore symmetry and distribution, as observed in the 3

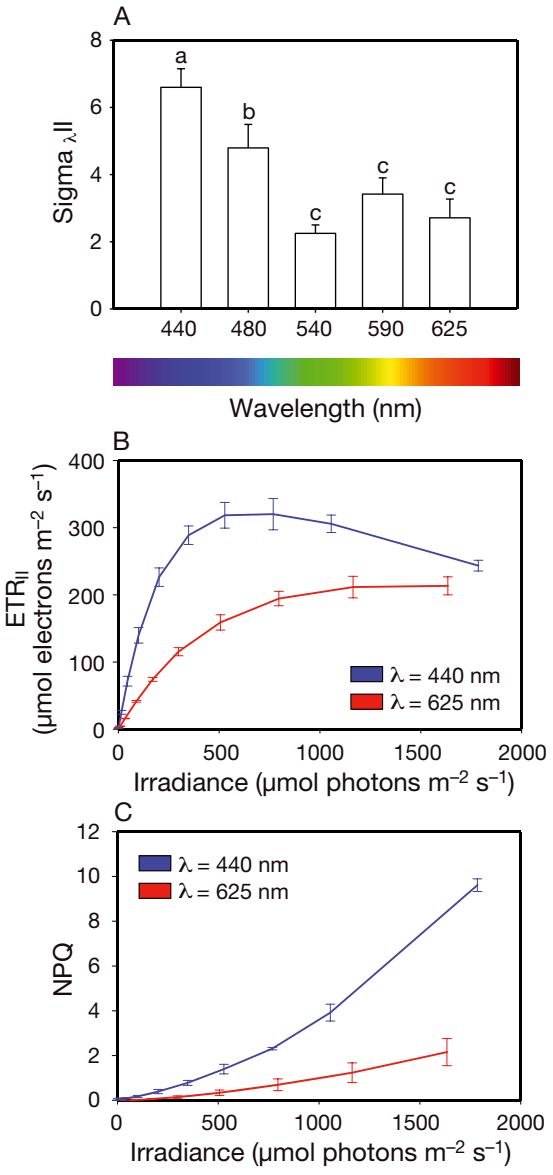

Fig. 4. Photosynthetic activity of raphid diatoms from an estuarine intertidal mudflat. (A) Functional wavelength-dependent absorption cross section of PSII ($Sigma_\lambda II$) determined at different colors in the visible spectrum of light. Significant differences (p = 0.05) are indicated by use of small letters. (B) Steady-state electron transport rates at PSII (ETR_{II}) measured as a function of photon irradiance and light color. (C) Non-photochemical energy quenching at PSII (NPQ) as a function of photon irradiance and light color

tested species, affects the valve photonic properties and causes photonic bandgaps. Further understanding of such phenomena would rely on a more detailed investigation of the valve ultrastructure, which is currently lacking, in combination with numerical simulations of the structure-light interactions (Russell 1992). Higher attenuation of blue light by diatom valves has been shown before, e.g. in the freshwater

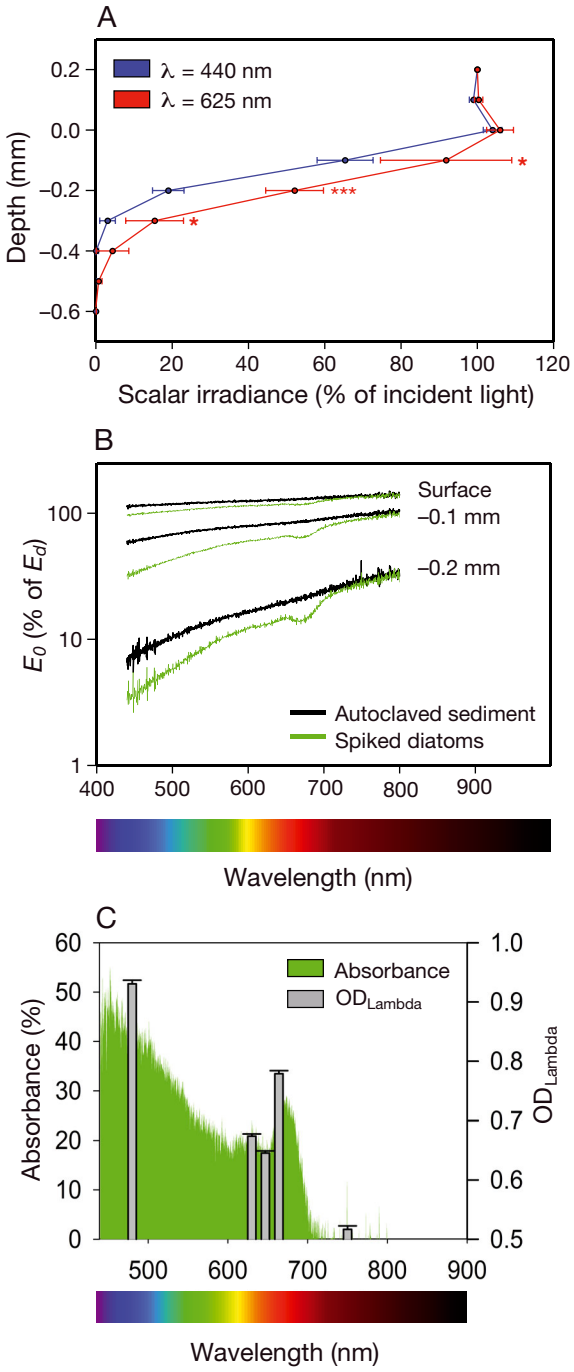

Fig. 5. Spectral attenuation of light in a diatom dominated intertidal estuarine mudflat. (A) Attenuation of blue and red scalar irradiance in autoclaved sediment. Asterisks indicate significance at the $p \leq 0.05$ (*), $p \leq 0.01$ (**), and $p \leq 0.001$ level (***). (B) Spectral scalar irradiance (E_0) in different depths normalized to the downwelling irradiance at the sediment surface (E_d), as measured in autoclaved sediment in the absence (Autoclaved sediment) and presence of diatoms (Spiked diatoms). (C) Light absorption spectrum of diatoms calculated as the ratio of scalar irradiance in autoclaved sediment with and without diatoms at 0.1 mm depth, respectively. The optical density (OD_{Lambda}) of a diatom suspension at different wavelengths is shown as bars

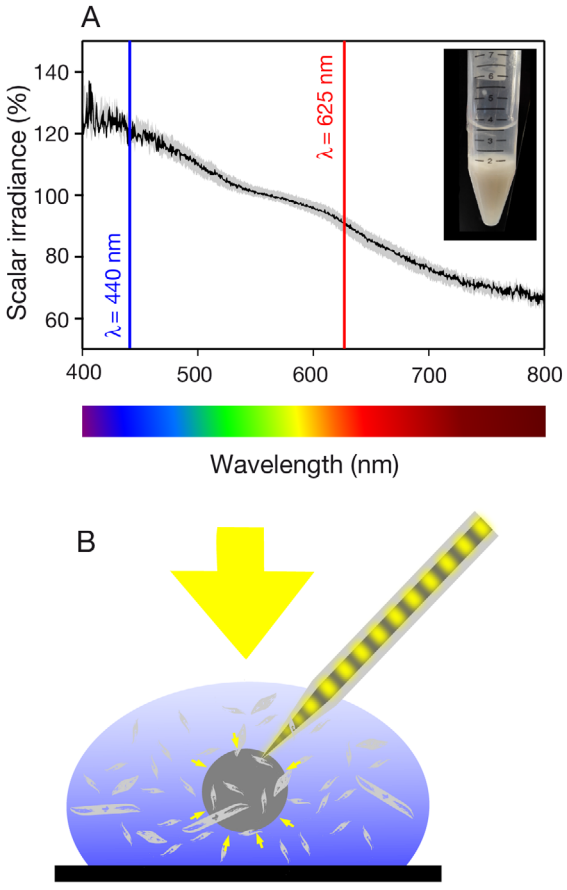

Fig. 6. Light enhancement by nanostructured frustules of raphid diatoms. (A) Spectral scalar irradiance measured in a water drop containing clean oxidized frustules of raphid diatoms collected from an intertidal estuarine mudflat. The inset shows the highly concentrated frustule slurry. (B) Schematic illustration of the setup: The light-collecting sphere (dark grey circle) of a scalar irradiance microprobe collected diffused light (small yellow arrows) scattered on the frustules from different raphid diatom species (light grey) placed in a drop of water (blue). The microprobe was inserted into the droplet at an angle of 45° relative to the vertically incident collimated white light (large yellow arrow)

diatom *Melosira varians*, where it was speculated that more energetic blue light could be absorbed by the biosilica of the valve in order to protect photosynthesis at high irradiance (Yamanaka et al. 2008). Valves of some diatoms can absorb wavelengths in the UV range (Ellegaard et al. 2016), while the amorphous silicate in the diatom frustule (Sumper 2002) is nearly transparent throughout the visible spectrum of light (Fanderlik 1983). Hence, attenuation of blue wavelengths is apparently caused by diffractive interactions of light with the photonic crystal-like structures of the valve wall (Hoover & Hoover 1970). Light can for example diffract on the network of pores on the valve surface (De Stefano et al. 2007;

Fig. 2C) or scatter on the complex silicate structures inside the valve wall (Hoover & Hoover 1970). Such scattering structures can be seen in dark field microscopy where direct illumination is blocked. We observed forward scattering of blue light on the valves in all tested species; however, the angle of incident white light at which this phenomenon was visible varied between the species (Fig. 3A). We speculate that the apparent conservation of blue light scattering observed on the valves of different species could indicate that this phenomenon has an ecological advantage for the diatom cell. This was further promoted by the observed variation of the effect dependent on the angle of light incidence, indicative for different light micro-environments inhabited by these species inside the microphytobenthos, where some species might locate at subsurface positions in diffused light fields (Baker & Lavelle 1984, Kühl & Jørgensen 1994), while other species might experience more collimated sunlight at the sediment surface (Kirk 2010). Different life-strategies might also be indicated by variation of the spatial distribution of photosynthetic compartments in the cell, i.e. number and arrangement of chloroplasts (Fig. 3B). In contrast, pelagic centric diatom species have multiple chloroplasts that are usually evenly distributed over the cell cortical periphery (Yogamoorthi 2007, Armbrecht et al. 2014, Goessling et al. 2016). The structural arrangement of chloroplasts might hence indicate different life-strategies in response to the respective light micro-environment. Links between light climate, life-strategy and the biochemical photosynthetic architecture of diatoms were proposed earlier by Strzepek & Harrison (2004), who observed that pelagic species have widely forfeit their photosynthetic flexibility to intermittent light regimes in order to reduce iron requirements. We speculate that the variation of valve optical properties and its underlying photonic crystal-like structures are indicative of different life-strategies of diatom species and furthermore that such structures promote photosynthesis at varying light environments. However, more detailed bio-optical studies at the single cell level are needed to unravel the exact optical mechanisms and their effect on diatom photosynthesis.

Absorption of light in diatoms is dependent on their photopigments, which typically absorb more light in the blue spectral range (Kuczynska et al. 2015). However, whether or not absorbed light is available for photosynthesis is dependent not only on the type and assembly of pigments at the photosystems but also on the antenna pigment-connectivity, which can be determined as the wavelength-dependent functional light absorption cross-section ($Sigma_{\lambda}II$; Schreiber et al. 2012). We confirmed earlier results observed in the centric diatom species *Coscinodiscus granii*, showing that $Sigma_{\lambda}II$ was significantly higher under blue light compared to under red light (Goessling et al. 2016; our Fig. 4A). Higher PSII electron transport rates (ETRII) at λ = 450 nm compared with rates induced by red light (Fig. 4B) may explain the higher diatom productivity when grown under blue light treatments, as observed in phytoplanktonic (Sanchez Saavedra & Voltolina 1995, Goessling et al. 2016) and benthic diatom species (Mercado et al. 2004). However, another study found that diatom growth rates in all 8 tested benthic species did not increase under blue light when compared to similar irradiances at other colors (Correa-Reyes et al. 2001). Mercado et al. (2004) therefore concluded that the effect of blue light on the growth of benthic diatoms could be species-dependent (Mercado et al. 2004). Energy dissipation by carotenoids can also reduce photosynthetic rates under blue light, which is energy-richer and usually more absorbed (Dougher & Bugbee 2001). We could confirm that blue light induced higher non-photochemical energy quenching (NPQ) compared to that induced by red light (of similar photon irradiance) in a suspension of benthic diatoms (Fig. 4C). Brunet et al. (2014) showed that the xanthophyll pool size and the NPQ amplitude increased when the pennate diatom species *Pseudonitzschia multistriata* was grown under blue light for several days (Brunet et al. 2014). Hence, the high response of NPQ under blue light observed in our samples may indicate that diatoms from the suspension were adapted to considerable amounts of blue light inside the sediment. Interestingly, we observed that although blue light attenuated more rapidly with depth (Fig. 5A), diatoms were able to harvest blue light more efficiently than longer wavelengths. Thus, a light absorption spectrum typical for diatoms was recorded *in vitro*, displaying the effective use of blue light by diatoms located at different depths (Fig. 5B,C). Rapid attenuation of blue light as observed in intertidal mudflats earlier (Cartaxana et al. 2016) could be linked to the fine sediment texture, i.e. shorter wavelengths might be scattered on particles of same or smaller size via Mie or Rayleigh scattering, respectively, in combination with strong absorption by organic debris (Kühl & Jørgensen 1994).

To investigate the potential implication of the optical properties of nanostructured diatom frustules upon the light field inside the sediment, we also measured attenuation of incident light in a drop of water containing slurry of oxidized frustules. Here,

blue light was significantly enhanced, which might indicate that the frustule optical properties could also modulate PAR on the community level inside the sedimentary biofilm (Fig. 6). Enhanced blue light might be explained by interactions of shorter wavelengths in the visible spectrum of light with the photonic-crystal like frustule structures or by Rayleigh scattering on subwavelengths frustule structures.

Stomp et al. (2007) point out that the specific sets of pigments that evolved on Earth can be regarded as instrumental for niche differentiation among phototrophs in relation to the solar spectrum as an energy resource, and such differentiation can lead to reduced competition and coexistence of species (Stomp et al. 2007). Selective filtration of sunlight by photopigments leaves out parts of the spectrum available for other phototrophic organisms. The canopies of rainforests (Endler 1993, Binkley et al. 2013) and stratified microbial mats (e.g. Kühl & Fenchel 2000) are well-studied examples of such efficient niche differentiation in regards to absorption and light use throughout the spectrum of sunlight. Biological photonic crystal structures, which are surprisingly widespread among photosynthetic organisms (Glover & Whitney 2010, Vignolini et al. 2013), could further broaden the spectral use of sunlight by local enhancement and redistribution of particular wavelength within the PAR range. Such optical modulation has e.g. been demonstrated in shade-dwelling *Begonia* spp. living on the floor of tropical forests, enhancing the quantum yield of PSII by increased light capture to the green spectral range of light (Jacobs et al. 2016). Photonic crystal structures might thus constitute an advantage in strongly light-limited environments, such as in diatom-dominated microphytobenthos (Watermann et al. 1999). Cyanobacteria, which often occur in combination with diatoms in intertidal mudflats (Underwood & Smith 1998, Stal 2010) may leave colorful niches by lower absorption in the blue-cyan spectral range of light (Nicklisch 1998), where rapid attenuation of these wavelengths inside the sediment might be compensated by photonic crystal structures in the frustule of raphid diatom species. However, we strongly encourage that further research needs to done to prove or disprove the contiguity of diatom frustule optical properties upon niche differentiation of diatoms in the microphytobenthos. Such experiments may focus on the biofilm structure in intertidal mudflats and on the behavioral light acclimation, including migration behavior, subsurface location and micro-cycling of single diatom species.

In conclusion, this first biophotonic study of pennate diatom frustules showed an apparent species-specific variation in the optical properties of photonic crystal-like structures in the valve. We speculate that such variation can facilitate niche differentiation inside the biofilm, and we propose that similar relationships might exist in other life-forms of diatoms. Although the frustule may be one outstanding example of structural light manipulation in nature, we propose that photonic structures can also be linked to niche differentiation and efficient photosynthesis in other phototrophic organisms. For now, we conclude that the optical properties of the frustule of diatoms modulate visible light in the PAR range inside the cell, and inside the sediment of an estuarine intertidal mudflat.

Acknowledgements. This study was funded by a Sapere-Aude Advanced grant from the Danish Council for Independent Research \ Natural Sciences (M.K.) and an instrument grant from the Carlsberg Foundation (M.K.). This work was also supported by the Fundação para a Ciência e a Tecnologia [doctoral fellowship SFRH/BD/86788/2012 to S.F.]. We thank Lars Rickelt (www.zenzor.eu) for providing custom-made fiber optic scalar irradiance microprobes. We acknowledge the assistance of William Schmidt during sediment sampling. We are grateful for fruitful discussions with Jörg Frommlet, Matthew Nitschke, João Simões, Gregor Christa and William Schmidt, and for the excellent technical support during the experimental work at the CESAM lab. We are furthermore obliged to Laetitia Carrive (Université Paris-Sud) for the discussion on bio-diversity which shaped the current manuscript.

LITERATURE CITED

Aitken ZH, Luo S, Reynolds SN, Thaulow C, Greer JR (2016) Microstructure provides insights into evolutionary design and resilience of *Coscinodiscus* sp. frustule. Proc Natl Acad Sci USA 113:2017–2022

Apel K, Hirt H (2004) Reactive oxygen species: metabolism, oxidative stress, and signal transduction. Annu Rev Plant Biol 55:373–399

Armbrecht LH, Smetacek V, Assmy P, Klaas C (2014) Cell death and aggregate formation in the giant diatom *Coscinodiscus wailesii* (Gran & Angst, 1931). J Exp Mar Biol Ecol 452:31–39

Atlas D, Bannister TT (1980) Dependence phytoplankton of mean spectral extinction coefficient on depth, water color, and species. Limnol Oceanogr 25:157–159

Babin M, Morel A, Fournier-Sicre V, Fell F, Stramski D (2003) Light scattering properties of marine particles in coastal and open ocean waters as related to the particle mass concentration. Limnol Oceanogr 48:843–859

Baker ET, Lavelle JW (1984) The effect of particle size on the light attenuation coefficient of natural suspensions. J Geophys Res 89:8197–8203

Bilger W, Björkman O (1990) Role of the xanthophyll cycle in photoprotection elucidated by measurements of light-

induced absorbance changes, fluorescence and photosynthesis in leaves of *Hedera canariensis*. Photosynth Res 25:173–185

Binkley D, Campoe OC, Gspaltl M, Forrester DI (2013) Light absorption and use efficiency in forests: why patterns differ for trees and stands. For Ecol Manage 288:5–13

Bobos I, Rocha F (2006) Radiocaesium dispersion and fixation in the lagoon systems of 'Ria de Aveiro', Portugal. J Geochem Explor 88:367–372

Boyd PW, Watson AJ, Law CS, Abraham ER and others (2000) A mesoscale phytoplankton bloom in the polar Southern Ocean stimulated by iron fertilization. Nature 407:695–702

Brunet C, Chandrasekaran R, Barra L, Giovagnetti V, Corato F, Ruban AV (2014) Spectral radiation dependent photoprotective mechanism in the diatom *Pseudo-nitzschia multistriata*. PLOS ONE 9:387015

Cartaxana P, Serôdio J (2008) Inhibiting diatom motility: a new tool for the study of the photophysiology of intertidal microphytobenthic biofilms. Limnol Oceanogr Methods 6:466–476

Cartaxana P, Ribeiro L, Goessling J, Cruz S, Kühl M (2016) Light and O_2 microenvironments in two contrasting diatom-dominated coastal sediments. Mar Ecol Prog Ser 545:35–47

Chen X, Wang C, Baker E, Sun C (2015) Numerical and experimental investigation of light trapping effect of nanostructured diatom frustules. Sci Rep 5:11977

Consalvey M, Paterson DM, Underwood GJC (2004) The ups and downs of life in a benthic biofilm: migration of benthic diatoms. Diatom Res 19:181–202

Correa-Reyes JG, Sanchez-Saavedra MP, Siqueiros-Beltrones DA, Flores-Acevedo N (2001) Isolation and growth of eight strains of benthic diatoms under two light conditions. J Shellfish Res 20:603–610

De Stefano L, Rea I, Rendina I, De Stefano M, Moretti L (2007) Lensless light focusing with the centric marine diatom *Coscinodiscus walesii*. Opt Express 15:18082–18088

De Tommasi E (2016) Light manipulation by single cells: the case of diatoms. J Spectrosc 2016:1–13

Demmig-Adams B, Adams WW (1992) Responses of plants to high light stress. Annu Rev Plant Physiol Plant Mol Biol 43:599–626

Dossou KB (2017) Large field enhancement obtained by combining Fabry-Perot resonance and Rayleigh anomaly in photonic crystal slabs. J Optics 19:45101

Dougher TA, Bugbee B (2001) Differences in the response of wheat, soybean and lettuce to reduced blue radiation. Photochem Photobiol 73:199–207

Edgar LA, Pickett-Heaps JD (1983) The mechanism of diatom locomotion. I. An ultrastructural study of the motility apparatus. Proc R Soc B 218:331–343

Ellegaard M, Lenau T, Lundholm N, Maibohm C and others (2016) The fascinating diatom frustule — Can it play a role for attenuation of UV radiation? J Appl Phycol 28: 3295–3306

Endler J (1993) The color of light in forests and its implications. Ecol Monogr 63:1–27

Fanderlik I (1983) Optical properties of glass. Glass Science and Technology, Vol. 5. Elsevier, Amsterdam, p 5–8

Fuhrmann T, Landwehr S, El Rharbi-Kucki M, Sumper M (2004) Diatoms as living photonic crystals. Appl Phys B 78:257–260

Genty B, Briantais JM, Baker NR (1989) The relationship between the quantum yield of photosynthetic electron transport and quenching of chlorophyll fluorescence. Biochim Biophys Acta, Gen Subj 990:87–92

Gilbert M, Wilhelm C, Richter M (2000) Bio-optical modelling of oxygen evolution using in vivo fluorescence: comparison of measured and calculated photosynthesis/irradiance (P-I) curves in four representative phytoplankton species. J Plant Physiol 157:307–314

Glover BJ, Whitney HM (2010) Structural colour and iridescence in plants: the poorly studied relations of pigment colour. Ann Bot 105:505–511

Goessling JW, Cartaxana P, Kühl M (2016) Photo-protection in the centric diatom *Coscinodiscus granii* is not controlled by chloroplast high-light avoidance movement. Front Mar Sci 2:1–10

Guiry MD (2012) How many species of algae are there? J Phycol 48:1057–1063

Hamm CE, Merkel R, Springer O, Jurkojc P, Maier C, Prechtel K, Smetacek V (2003) Architecture and material properties of diatom shells provide effective mechanical protection. Nature 421:841–843

Haupt W (1973) Role of light in chloroplast movement. Bioscience 23:289–296

Holt AL, Vahidinia S, Gagnon YL, Morse DE, Sweeney AM (2014) Photosymbiotic giant clams are transformers of solar flux. J R Soc Interface 11:20140678

Hoover RB, Hoover MJ (1970) Optical phenomena in diatoms. Arkansas Acad Sci Proc 1:8–10

Ingalls AE, Whitehead K, Bridoux MC (2010) Tinted windows: the presence of the UV absorbing compounds called mycosporine-like amino acids embedded in the frustules of marine diatoms. Geochim Cosmochim Acta 74:104–115

Jacobs M, Lopez-garcia M, Phrathep OP, Lawson T (2016) Photonic crystal structure of *Begonia* chloroplasts enhances photosynthetic efficiency. Nat Plants 2:16162

Kinoshita S, Yoshioka S, Miyazaki J (2008) Physics of structural colors. Rep Prog Phys 71:076401

Kirk JTO (2010) Light and photosynthesis in aquatic ecosystems. Cambridge University Press, Cambridge

Kuczynska P, Jemiola-Rzeminska M, Strzalka K (2015) Photosynthetic pigments in diatoms. Mar Drugs 13:5847–5881

Kühl M, Fenchel T (2000) Bio-optical characteristics and the vertical distribution of photosynthetic pigments and photosynthesis in an artificial cyanobacterial mat. Microb Ecol 40:94–103

Kühl M, Jørgensen BB (1994) The light-field of microbenthic communities- radiance distribution and microscale optics of sandy coastal sediments. Limnol Oceanogr 39: 1368–1398

Kühl M, Lassen C, Jørgensen BB (1994) Light penetration and light intensity in sandy marine sediments measured with irradiance and scalar irradiance fiber-optic microprobes. Mar Ecol Prog Ser 105:139–148

Lavaud J (2007) Fast regulation of photosynthesis in diatoms: mechanisms, evolution and ecophysiology. Funct Plant Sci Biotechonol 1:267–287

Losic D, Rosengarten G, Mitchell JG, Voelcker NH (2006) Pore architecture of diatom frustules: potential nanostructured membranes for molecular and particle separations. J Nanosci Nanotech 6:982–989

Mann J, Myers J (1968) On pigments, growth, and photosynthesis of *Phaedactylum tricornutum*. J Phycol 4: 349–355

Max NL (1986) Light diffusion through clouds and haze. Comput Vis Graph Image Process 33:280–292

Maxwell K, Johnson GN (2000) Chlorophyll fluorescence — a practical guide. J Exp Bot 51:659–668

Mercado JM, Sánchez-Saavedra MDP, Correa-Reyes G, Lubián L, Montero O, Figueroa FL (2004) Blue light effect on growth, light absorption characteristics and photosynthesis of five benthic diatom strains. Aquat Bot 78:265–277

Milligan AJ (2002) A proton buffering role for silica in diatoms. Science 297:1848–1850

Mock T, Valentin K (2004) Photosynthesis and cold acclimation: molecular evidence from a polar diatom. J Phycol 40:732–741

Mortain-Bertrand A (1989) Effects of light fluctuations on the growth and productivity of Antarctic diatoms in culture. Polar Biol 9:245–252

Nicklisch A (1998) Growth and light absorption of some planktonic cyanobacteria, diatoms and Chlorophyceae under simulated natural light fluctuations. J Plankton Res 20:105–119

Rickelt LF, Lichtenberg M, Trampe ECL, Kühl M (2016) Fiber-optic probes for small-scale measurements of scalar irradiance. Photochem Photobiol 92:331–342

Romann J, Valmalette JC, Chauton MS, Tranell G, Einarsrud MA, Vadstein O (2015) Wavelength and orientation dependent capture of light by diatom frustule nanostructures. Sci Rep 5:17403

Round FE, Crawford RM, Mann DG (1990) The diatoms: biology and morphology of the genera. Cambridge University Press, Cambridge

Ruban A, Lavaud J, Rousseau B, Guglielmi G, Horton P, Etienne AL (2004) The super-excess energy dissipation in diatom algae: comparative analysis with higher plants. Photosynth Res 82:165–175

Russell PSJ (1992) Photonic band gaps. Phys World 5:37–42

Sanchez Saavedra MP, Voltolina D (1995) The effect of different light quality on the food value of the diatom *Chaetoceros* sp. for *Artemia franciscana*. Riv Ital Acquacolt 30:135–138

Schenck HJ (1957) On the focusing of sunlight by ocean waves. J Opt Soc Am 47:653–657

Schindelin J, Arganda-Carreras I, Frise E, Kaynig V and others (2012) Fiji: an open-source platform for biological-image analysis. Nat Methods 9:676–682

Schreiber U, Klughammer C, Kolbowski J (2012) Assessment of wavelength-dependent parameters of photosynthetic electron transport with a new type of multicolor PAM chlorophyll fluorometer. Photosynth Res 113: 127–144

Schumann A, Goss R, Jakob T, Wilhelm C (2007) Investigation of the quenching efficiency of diatoxanthin in cells of *Phaeodactylum tricornutum* (Bacillariophyceae) with different pool sizes of xanthophyll cycle pigments. Phycologia 46:113–117

Serôdio J, Vieira S, Cruz S (2008) Photosynthetic activity, photoprotection and photoinhibition in intertidal microphytobenthos as studied in situ using variable chlorophyll fluorescence. Cont Shelf Res 28:1363–1375

Serôdio J, Schmidt W, Frankenbach S (2017) A chlorophyll fluorescence-based method for the integrated characterization of the photophysiological response to light stress. J Exp Bot 68:1123–1135

Siefermann-Harms D (1987) The light-harvesting and protective functions of carotenoids in photosynthetic membranes. Physiol Plant 69:561–568

Smetacek VS (1985) Role of sinking in diatom life-history: ecological, evolutionary and geological significance. Mar Biol 84:239–251

Stal LJ (2010) Microphytobenthos as a biogeomorphological force in intertidal sediment stabilization. Ecol Eng 36: 236–245

Stomp M, Huisman J, Stal LJ, Matthijs HCP (2007) Colorful niches of phototrophic microorganisms shaped by vibrations of the water molecule. ISME J 1:271–282

Strzepek RF, Harrison PJ (2004) Photosynthetic architecture differs in coastal and oceanic diatoms. Nature 431: 689–692

Sumper M (2002) A phase separation model for the nanopatterning of diatom biosilica. Science 295:2430–2433

Sun J, Bhushan B, Tong J (2013) Structural coloration in nature. RSC Advances 3:14862–14889

Thomas DN, Dieckmann GS (2002) Antarctic Sea ice — a habitat for extremophiles. Science 295:641–644

Trampe E, Kolbowski J, Schreiber U, Kühl M (2011) Rapid assessment of different oxygenic phototrophs and single-cell photosynthesis with multicolour variable chlorophyll fluorescence imaging. Mar Biol 158:1667–1675

Underwood GJC, Smith DJ (1998) Predicting epipelic diatom exopolymer concentrations in intertidal sediments from sediment chlorophyll *a*. Microb Ecol 35:116–125

Valmalette J, Romann J, Røyset A, Einarsrud M (2015) 3D-hyperspectral mapping of light propagation through diatom frustule silica nanostructures. Opt Lett 40:3–5

Vanormelingen P, Verleyen E, Vyverman W (2008) The diversity and distribution of diatoms: from cosmopolitanism to narrow endemism. Biodivers Conserv 17: 393–405

Vignolini S, Moyroud E, Glover BJ, Steiner U, Glover BJ (2013) Analysing photonic structures in plants. J R Soc Interface 10:20130394

Watermann F, Hillebrand H, Gerdes G, Krumbein WE, Sommer U (1999) Competition between benthic cyanobacteria and diatoms as influenced by different grain sizes and temperatures. Mar Ecol Prog Ser 187:77–87

Witkowski A, Lange-Bertalot HMD (2000) Diatom flora of marine coasts. In: Lange-Bertalot H (ed) Iconographia Diatomologica: annotated diatom micrographs, Vol. 28. Koeltz Scientific Books, Oberreifenberg

Wu J, Neimanis S, Heber U (1991) Photorespiration is more effective than the Mehler reaction in protecting the photosynthetic apparatus against photoinhibition. Bot Acta 104:283–291

Yamanaka S, Yano R, Usami H, Hayashida N, Ohguchi M, Takeda H, Yoshino K (2008) Optical properties of diatom silica frustule with special reference to blue light. J Appl Phys 103:074701

Yogamoorthi A (2007) Artificial UV-B induced changes in pigmentation of marine diatom *Coscinodiscus gigas*. J Environ Biol 28:327–330

Zhu SH, Green BR (2010) Photoprotection in the diatom *Thalassiosira pseudonana*: role of LI818-like proteins in response to high light stress. Biochim Biophys Acta BBABioenerg 1797:1449–1457

Editorial responsibility: Steven Lohrenz, New Bedford, Massachusetts, USA

Submitted: June 15, 2017; Accepted: December 14, 2017
Proofs received from author(s): February 1, 2018